

Measurements of the observed cross sections for exclusive light hadron production in e^+e^- annihilation at $\sqrt{s} = 3.773$ and 3.650 GeV

BES Collaboration

M. Ablikim¹, J. Z. Bai¹, Y. Ban¹², X. Cai¹, H. F. Chen¹⁶, H. S. Chen¹, H. X. Chen¹, J. C. Chen¹, Jin Chen¹, Y. B. Chen¹, Y. P. Chu¹, Y. S. Dai¹⁸, L. Y. Diao⁹, Z. Y. Deng¹, Q. F. Dong¹⁵, S. X. Du¹, J. Fang¹, S. S. Fang^{1a}, C. D. Fu¹⁵, C. S. Gao¹, Y. N. Gao¹⁵, S. D. Gu¹, Y. T. Gu⁴, Y. N. Guo¹, K. L. He¹, M. He¹³, Y. K. Heng¹, J. Hou¹¹, H. M. Hu¹, J. H. Hu³, T. Hu¹, X. T. Huang¹³, X. B. Ji¹, X. S. Jiang¹, X. Y. Jiang⁵, J. B. Jiao¹³, D. P. Jin¹, S. Jin¹, Y. F. Lai¹, G. Li^{1b}, H. B. Li¹, J. Li¹, R. Y. Li¹, S. M. Li¹, W. D. Li¹, W. G. Li¹, X. L. Li¹, X. N. Li¹, X. Q. Li¹¹, Y. F. Liang¹⁴, H. B. Liao¹, B. J. Liu¹, C. X. Liu¹, F. Liu⁶, Fang Liu¹, H. H. Liu¹, H. M. Liu¹, J. Liu^{12c}, J. B. Liu¹, J. P. Liu¹⁷, Jian Liu¹, Q. Liu¹, R. G. Liu¹, Z. A. Liu¹, Y. C. Lou⁵, F. Lu¹, G. R. Lu⁵, J. G. Lu¹, C. L. Luo¹⁰, F. C. Ma⁹, H. L. Ma², L. L. Ma^{1d}, Q. M. Ma¹, Z. P. Mao¹, X. H. Mo¹, J. Nie¹, R. G. Ping¹, N. D. Qi¹, H. Qin¹, J. F. Qiu¹, Z. Y. Ren¹, G. Rong¹, X. D. Ruan⁴, L. Y. Shan¹, L. Shang¹, D. L. Shen¹, X. Y. Shen¹, H. Y. Sheng¹, H. S. Sun¹, S. S. Sun¹, Y. Z. Sun¹, Z. J. Sun¹, X. Tang¹, G. L. Tong¹, D. Y. Wang^{1e}, L. Wang¹, L. L. Wang¹, L. S. Wang¹, M. Wang¹, P. Wang¹, P. L. Wang¹, Y. F. Wang¹, Z. Wang¹, Z. Y. Wang¹, Zheng Wang¹, C. L. Wei¹, D. H. Wei¹, Y. Weng¹, N. Wu¹, X. M. Xia¹, X. X. Xie¹, G. F. Xu¹, X. P. Xu⁶, Y. Xu¹¹, M. L. Yan¹⁶, H. X. Yang¹, Y. X. Yang³, M. H. Ye², Y. X. Ye¹⁶, G. W. Yu¹, C. Z. Yuan¹, Y. Yuan¹, S. L. Zang¹, Y. Zeng⁷, B. X. Zhang¹, B. Y. Zhang¹, C. C. Zhang¹, D. H. Zhang¹, H. Q. Zhang¹, H. Y. Zhang¹, J. W. Zhang¹, J. Y. Zhang¹, S. H. Zhang¹, X. Y. Zhang¹³, Yiyun Zhang¹⁴, Z. X. Zhang¹², Z. P. Zhang¹⁶, D. X. Zhao¹, J. W. Zhao¹, M. G. Zhao¹, P. P. Zhao¹, W. R. Zhao¹, Z. G. Zhao^{1f}, H. Q. Zheng¹², J. P. Zheng¹, Z. P. Zheng¹, L. Zhou¹, K. J. Zhu¹, Q. M. Zhu¹, Y. C. Zhu¹, Y. S. Zhu¹, Z. A. Zhu¹, B. A. Zhuang¹, X. A. Zhuang¹, B. S. Zou¹

¹ *Institute of High Energy Physics, Beijing 100049, People's Republic of China*

² *China Center for Advanced Science and Technology (CCAST), Beijing 100080, People's Republic of China*

³ *Guangxi Normal University, Guilin 541004, People's Republic of China*

⁴ *Guangxi University, Nanning 530004, People's Republic of China*

⁵ *Henan Normal University, Xinxiang 453002, People's Republic of China*

⁶ *Huazhong Normal University, Wuhan 430079, People's Republic of China*

⁷ *Hunan University, Changsha 410082, People's Republic of China*

⁸ *Jinan University, Jinan 250022, People's Republic of China*

⁹ *Liaoning University, Shenyang 110036, People's Republic of China*

¹⁰ *Nanjing Normal University, Nanjing 210097, People's Republic of China*

¹¹ *Nankai University, Tianjin 300071, People's Republic of China*

¹² *Peking University, Beijing 100871, People's Republic of China*

¹³ *Shandong University, Jinan 250100, People's Republic of China*

¹⁴ *Sichuan University, Chengdu 610064, People's Republic of China*

¹⁵ *Tsinghua University, Beijing 100084, People's Republic of China*

¹⁶ *University of Science and Technology of China, Hefei 230026, People's Republic of China*

¹⁷ *Wuhan University, Wuhan 430072, People's Republic of China*

¹⁸ *Zhejiang University, Hangzhou 310028, People's Republic of China*

^a *Current address: DESY, D-22607, Hamburg, Germany*

^b *Current address: Universite Paris XI, LAL-Bat. 208-BP34, 91898-ORSAY Cedex, France*

^c *Current address: Max-Planck-Institut fuer Physik, Foehringer Ring 6, 80805 Munich, Germany*

^d *Current address: University of Toronto, Toronto M5S 1A7, Canada*

^e *Current address: CERN, CH-1211 Geneva 23, Switzerland*

^f *Current address: University of Michigan, Ann Arbor, MI 48109, USA**

By analyzing the data sets of 17.3 pb^{-1} taken at $\sqrt{s} = 3.773 \text{ GeV}$ and 6.5 pb^{-1} taken at $\sqrt{s} = 3.650 \text{ GeV}$ with the BESII detector at the BEPC collider, we have measured the observed cross sections for 12 exclusive light hadron final states produced in e^+e^- annihilation at the two energy points. We have also set the upper limits on the observed cross sections and the branching fractions for $\psi(3770)$ decay to these final states at 90% C.L.

I. INTRODUCTION

As the lowest mass charmonium resonance above the $D\bar{D}$ threshold, the $\psi(3770)$ is expected to decay almost entirely into pure $D\bar{D}$ pairs. However, there has been a “long-standing puzzle” that the $\psi(3770)$ is not saturated by $D\bar{D}$ decays [1]. Recently, CLEO Collaboration measured the $e^+e^- \rightarrow \psi(3770) \rightarrow \text{non-}D\bar{D}$ cross section to be $(-0.01 \pm 0.08_{-0.30}^{+0.41})$ nb [2]. While, BES Collaboration measured the branching fraction for $\psi(3770) \rightarrow \text{non-}D\bar{D}$ decay to be $(15 \pm 5)\%$ [3, 4, 5], which implies that the $\psi(3770)$ may substantially decay into charmless final states. Meanwhile many measurements about exclusive $\psi(3770) \rightarrow \text{non-}D\bar{D}$ decays are reported by BES [6, 7, 8, 9, 10] and CLEO [11, 12, 13, 14, 15, 16] Collaborations. However, these results can not explain the discrepancy between the observed cross sections $\sigma_{D\bar{D}}^{\text{obs}}$ and $\sigma_{\psi(3770)}^{\text{obs}}$ for $D\bar{D}$ and $\psi(3770)$ production. To understand the discrepancy, one may directly compare the observed cross sections for more exclusive light hadron final states at the center-of-mass energies at 3.773 GeV and below 3.660 GeV, excluding the contributions from J/ψ and $\psi(3686)$ due to ISR (Initial State Radiation) returns as well as $D\bar{D}$ decays. From these cross sections, one can also obtain some valuable information to understand the mechanism of the continuum light hadron production.

Following Ref. [10], we report measurements of the observed cross sections for the exclusive light hadron final states of $K^+K^-2(\pi^+\pi^-)$, $2(K^+K^-)\pi^+\pi^-$, $p\bar{p}2(\pi^+\pi^-)$, $4(\pi^+\pi^-)$, $K^+K^-2(\pi^+\pi^-)\pi^0$, $4(\pi^+\pi^-)\pi^0$, $\rho^0\pi^+\pi^-$, $\rho^0K^+K^-$, $\rho^0p\bar{p}$, $K^{*0}K^-\pi^+ + c.c.$, $\Lambda\bar{\Lambda}$ and $\Lambda\bar{\Lambda}\pi^+\pi^-$ produced in e^+e^- annihilation at $\sqrt{s} = 3.773$ and 3.650 GeV in this Letter. The measurements are made by analyzing the data sets of 17.3 pb^{-1} taken at $\sqrt{s} = 3.773$ GeV and 6.5 pb^{-1} taken at $\sqrt{s} = 3.650$ GeV with the BESII detector at the BEPC collider. For convenience, we call these two data sets to be the $\psi(3770)$ resonance data and the continuum data in the Letter, respectively.

II. BESII DETECTOR

The BESII is a conventional cylindrical magnetic detector that is described in detail in Refs. [17, 18]. A 12-layer Vertex Chamber (VC) surrounding a beryllium beam pipe provides input to event trigger, as well as coordinate information. A forty-layer main drift chamber (MDC) located just outside the VC yields precise measurements of charged particle trajectories with a solid angle coverage of 85% of 4π ; it also provides ionization energy loss (dE/dx) measurements for particle identification. Momentum resolution of $1.7\%\sqrt{1+p^2}$ (p

in GeV/c) and dE/dx resolution of 8.5% for Bhabha scattering electrons are obtained for the data taken at $\sqrt{s} = 3.773$ GeV. An array of 48 scintillation counters surrounding the MDC measures time of flight (TOF) of charged particles with a resolution of about 180 ps for electrons. Outside the TOF counters, a 12 radiation length, lead-gas barrel shower counter (BSC), operating in limited streamer mode, measures the energies of electrons and photons over 80% of the total solid angle with an energy resolution of $\sigma_E/E = 0.22/\sqrt{E}$ (E in GeV) and spatial resolutions of $\sigma_\phi = 7.9$ mrad and $\sigma_Z = 2.3$ cm for electrons. A solenoidal magnet outside the BSC provides a 0.4 T magnetic field in the central tracking region of the detector. Three double-layer muon counters instrument the magnet flux return and serve to identify muons with momentum greater than 500 MeV/c. They cover 68% of the total solid angle.

III. EVENT SELECTION

We reconstruct $e^+e^- \rightarrow$ exclusive light hadrons mentioned above by selecting the final states $m(\pi^+\pi^-)n(K^+K^-)i(p\bar{p})j(\gamma\gamma)$ ($m = 1, 2, 4$; $n = 0, 1, 2$; $i = 0, 1$ and $j = 0, 1$) from the data. For the processes containing π^0 , ρ^0 , K^{*0} and Λ mesons in the final states, we reconstruct these intermediate resonances by the decays $\pi^0 \rightarrow \gamma\gamma$, $\rho^0 \rightarrow \pi^+\pi^-$, $K^{*0} \rightarrow K^+\pi^-$ and $\Lambda \rightarrow p\pi^-$, respectively. For the decays $K^{*0} \rightarrow K^+\pi^-$ and $\Lambda \rightarrow p\pi^-$, charge conjugation is implied throughout the Letter.

To select good candidate events, we require that at least four charged tracks be well reconstructed in the MDC with good helix fits, and each of them be within $|\cos\theta| < 0.85$, where θ is the polar angle. All charged tracks, save those from the Λ decays, are required to originate from the interaction region $V_{xy} < 2.0$ cm and $|V_z| < 20.0$ cm, while those from the Λ decays are required to originate from the interaction region $V_{xy} < 8.0$ cm and $|V_z| < 20.0$ cm, where V_{xy} and $|V_z|$ are the closest approaches of the charged track in the xy -plane and z direction, respectively.

The charged particles are identified with the dE/dx and TOF measurements, with which the combined confidence levels (CL_π , CL_K and CL_p) for pion, kaon and proton hypotheses are calculated. The pion, kaon and proton candidates are required to satisfy $CL_\pi > 0.001$, $CL_K > CL_\pi$ and $\frac{CL_p}{CL_\pi + CL_K + CL_p} > 0.6$, respectively.

The good photon candidates are selected with the BSC measurements by the following criteria: the energy of the photon deposited in the BSC is greater than 50 MeV, the electromagnetic shower starts in the first 5 readout layers, the angle between the photon and the nearest charged track is greater than 22° [19], the opening angle between the cluster development direction and the photon emission direction is less than 37° [19].

In each event, several different charged track and/or neutral particle combinations may satisfy the above se-

*Electronic address: mabl@mail.ibep.ac.cn (H. J. Ma)

lection criteria for each exclusive light hadron final state. Each combination is imposed on an energy-momentum conservation kinematic fit. Only those combinations with a kinematic fit probability greater than 1% are accepted. If more than one combination satisfies the selection criteria in an event, only the combination with the largest fit probability is retained.

For the $2(\pi^+\pi^-)$ final state, we veto the background events of $(\gamma)J/\psi\pi^+\pi^-$ with $J/\psi \rightarrow \mu^+\mu^-$ by requiring that the invariant mass of any $\pi^+\pi^-$ combination be less than $3.00 \text{ GeV}/c^2$, where $\mu^+\mu^-$ pairs may be misidentified as $\pi^+\pi^-$ pairs.

For the $K^+K^-\pi^+\pi^-$, or $K^+K^-2(\pi^+\pi^-)[\pi^0]$ final state, we exclude the events from $D\bar{D}$ decays by rejecting those in which the D and \bar{D} mesons can be reconstructed in the decay modes of $D^0 \rightarrow K^-\pi^+$ and $\bar{D}^0 \rightarrow K^+\pi^-$, or $D^0 \rightarrow K^-\pi^+[\pi^0]$ and $\bar{D}^0 \rightarrow K^+\pi^-\pi^-\pi^+$, or $D^+ \rightarrow K^-\pi^+\pi^+[\pi^0]$ and $D^- \rightarrow K^+\pi^-\pi^-$, here charge conjugation is implied [20]. The contribution from other D meson decay modes is accounted by using Monte Carlo simulation, as discussed in Section V.

IV. DATA ANALYSIS

To study the final states $K^+K^-2(\pi^+\pi^-)$, $2(K^+K^-)\pi^+\pi^-$, $p\bar{p}2(\pi^+\pi^-)$ and $4(\pi^+\pi^-)$, we define a kinematic quantity of the scaled energy as $E_{\text{msr}}/E_{\text{cm}}$ [10]. Here, E_{msr} is the total originally measured energy of all the observed particles, and E_{cm} is the nominal center-of-mass energy. To look for possible intermediate resonances, we examine the invariant mass spectra of the $\gamma\gamma$, $\pi^+\pi^-$, $K^\pm\pi^\mp$ and $p\pi^-/\bar{p}\pi^+$ combinations from the selected $K^+K^-2(\pi^+\pi^-)\gamma\gamma$, $4(\pi^+\pi^-)\gamma\gamma$, $2(\pi^+\pi^-)$, $K^+K^-\pi^+\pi^-$, $p\bar{p}\pi^+\pi^-$ and $p\bar{p}2(\pi^+\pi^-)$ events. In the Letter, they are denoted by $M_{\gamma\gamma}$, $M_{\pi^+\pi^-}$, $M_{K^\pm\pi^\mp}$ and $M_{p\pi^-/\bar{p}\pi^+}$, respectively.

A. Candidates for $e^+e^- \rightarrow K^+K^-2(\pi^+\pi^-)$, $e^+e^- \rightarrow 2(K^+K^-)\pi^+\pi^-$, $e^+e^- \rightarrow p\bar{p}2(\pi^+\pi^-)$ and $e^+e^- \rightarrow 4(\pi^+\pi^-)$

Figure 1 shows the resulting $E_{\text{msr}}/E_{\text{cm}}$ distributions, with each peak centered around unity correctly, from the candidates for $e^+e^- \rightarrow K^+K^-2(\pi^+\pi^-)$, $e^+e^- \rightarrow 2(K^+K^-)\pi^+\pi^-$, $e^+e^- \rightarrow p\bar{p}2(\pi^+\pi^-)$ and $e^+e^- \rightarrow 4(\pi^+\pi^-)$. Fitting to the spectrum in each figure with a Gaussian function for the signal and a flat background yields the number N^{obs} of the signal events for each final state observed from the $\psi(3770)$ resonance data and the continuum data. However, there are only a few events in Figs. 1(b) and 1(b'). The mass window of $\pm 3\sigma_{E_{\text{msr}}/E_{\text{cm}}}$ around the nominal $E_{\text{msr}}/E_{\text{cm}}$ is taken as the $2(K^+K^-)\pi^+\pi^-$ signal region, where $\sigma_{E_{\text{msr}}/E_{\text{cm}}}$ is the resolution of the $E_{\text{msr}}/E_{\text{cm}}$ distribution determined by Monte Carlo simulation. The pairs of arrows in the figures show the $2(K^+K^-)\pi^+\pi^-$ signal regions. In the

signal regions, there are 5 and 2 signal events for the $2(K^+K^-)\pi^+\pi^-$ final state observed from the $\psi(3770)$ resonance data and the continuum data, respectively.

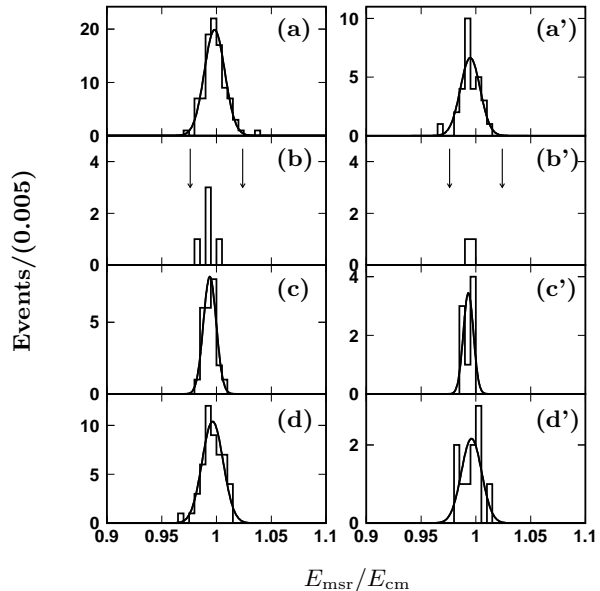


Fig. 1: The $E_{\text{msr}}/E_{\text{cm}}$ distributions of the candidates for (a) $e^+e^- \rightarrow K^+K^-2(\pi^+\pi^-)$, (b) $e^+e^- \rightarrow 2(K^+K^-)\pi^+\pi^-$, (c) $e^+e^- \rightarrow p\bar{p}2(\pi^+\pi^-)$ and (d) $e^+e^- \rightarrow 4(\pi^+\pi^-)$ selected from the $\psi(3770)$ resonance data (left) and the continuum data (right), where the pairs of arrows show the signal regions.

B. Candidates for $e^+e^- \rightarrow K^+K^-2(\pi^+\pi^-)\pi^0$ and $e^+e^- \rightarrow 4(\pi^+\pi^-)\pi^0$

Figure 2 shows the distributions of the invariant masses of the $\gamma\gamma$ combinations from the candidates for $e^+e^- \rightarrow K^+K^-2(\pi^+\pi^-)\pi^0$ and $e^+e^- \rightarrow 4(\pi^+\pi^-)\pi^0$. In Fig. 2(a), a π^0 signal is clearly observed. Fitting to the invariant mass spectrum with a Gaussian function for the π^0 signal and a flat background yields 21.3 ± 5.0 signal events for $e^+e^- \rightarrow K^+K^-2(\pi^+\pi^-)\pi^0$ observed from the $\psi(3770)$ resonance data. In the other figures, only a few events are observed, the mass window of $\pm 3\sigma_{M_{\gamma\gamma}}$ around the π^0 nominal mass is taken as the π^0 signal region, where $\sigma_{M_{\gamma\gamma}}$ is the π^0 mass resolution determined by Monte Carlo simulation. In Fig. 2(a'), there are 6(2) events observed in the signal region (the outside of the signal region). By assuming that the distribution of background is flat, 0.6 ± 0.4 background event in the signal region is estimated. After subtracting the background, we obtain 5.4 ± 2.5 signal events for $e^+e^- \rightarrow K^+K^-2(\pi^+\pi^-)\pi^0$ observed from the continuum data. In Figs. 2(b) and 2(b'), counting the events with $M_{\gamma\gamma}$ within the π^0 signal region, we obtain the numbers N^{obs} of the candidates for $e^+e^- \rightarrow 4(\pi^+\pi^-)\pi^0$ from the $\psi(3770)$ resonance data and the continuum data, respec-

tively.

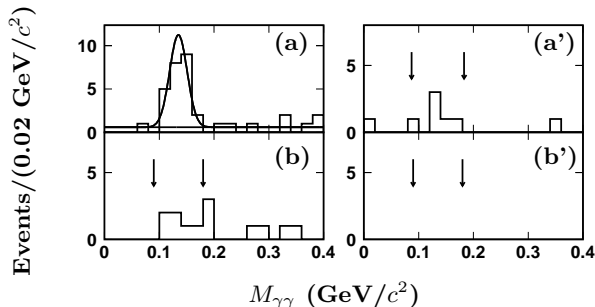


Fig. 2: The distributions of the invariant masses of the $\gamma\gamma$ combinations from the candidates for (a) $e^+e^- \rightarrow K^+K^-2(\pi^+\pi^-)\pi^0$ and (b) $e^+e^- \rightarrow 4(\pi^+\pi^-)\pi^0$ selected from the $\psi(3770)$ resonance data (left) and the continuum data (right), where the pairs of arrows indicate the π^0 signal regions.

C. Candidates for $e^+e^- \rightarrow \rho^0\pi^+\pi^-$, $e^+e^- \rightarrow \rho^0K^+K^-$ and $e^+e^- \rightarrow \rho^0p\bar{p}$

To investigate the processes $e^+e^- \rightarrow \rho^0\pi^+\pi^-$, $e^+e^- \rightarrow \rho^0K^+K^-$ and $e^+e^- \rightarrow \rho^0p\bar{p}$, we analyze the invariant mass spectra of the $\pi^+\pi^-$ combinations from the selected $2(\pi^+\pi^-)$, $\pi^+\pi^-K^+K^-$ and $\pi^+\pi^-p\bar{p}$ events, as shown in Fig. 3. The ρ^0 production can be observed in each figure. Fitting to these invariant mass spectra with a Breit-Wigner function convoluted with a Gaussian resolution function for the ρ^0 signal and a polynomial for the background, we obtain the numbers N^{obs} of the signal events for $e^+e^- \rightarrow \rho^0\pi^+\pi^-$, $e^+e^- \rightarrow \rho^0K^+K^-$ and $e^+e^- \rightarrow \rho^0p\bar{p}$ observed from the $\psi(3770)$ resonance data and the continuum data. In the fit, the mass and width of ρ^0 are fixed to the world averaged values from PDG [21].

D. Candidates for $e^+e^- \rightarrow K^{*0}K^-\pi^+ + c.c.$

To study the final state $e^+e^- \rightarrow K^{*0}K^-\pi^+ + c.c.$, we analyze the invariant mass spectra of the $K^\pm\pi^\mp$ combinations from the selected $K^+K^-\pi^+\pi^-$ events, as shown in Fig. 4. In each figure, the K^{*0} signal is clearly observed. Fitting to these invariant mass spectra with a Breit-Wigner function convoluted with a Gaussian resolution function for the K^{*0} signal and a second order polynomial for the background, we obtain the numbers N^{obs} of the signal events for $e^+e^- \rightarrow K^{*0}K^-\pi^+ + c.c.$ observed from the $\psi(3770)$ resonance data and the continuum data. In the fit, the mass and width of K^{*0} are fixed to the world averaged values from PDG [21].

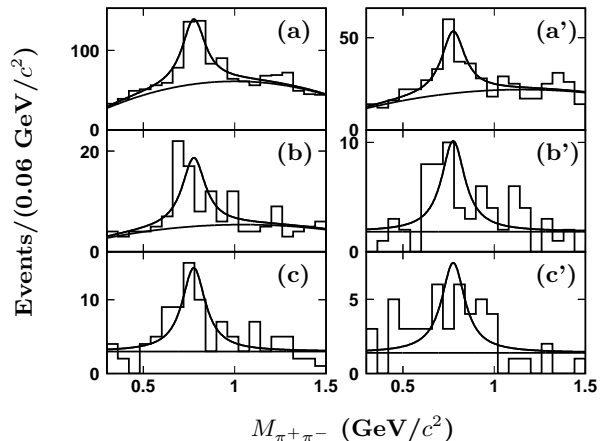


Fig. 3: The distributions of the invariant masses of the $\pi^+\pi^-$ combinations from the selected (a) $2(\pi^+\pi^-)$, (b) $K^+K^-\pi^+\pi^-$ and (c) $p\bar{p}\pi^+\pi^-$ events from the $\psi(3770)$ resonance data (left) and the continuum data (right).

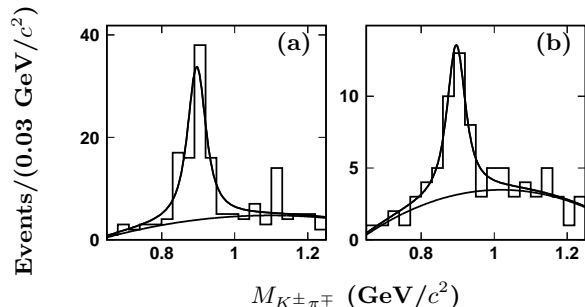


Fig. 4: The distributions of the invariant masses of the $K^\pm\pi^\mp$ combinations from the selected $K^+K^-\pi^+\pi^-$ events (a) from the $\psi(3770)$ resonance data and (b) from the continuum data.

E. Candidates for $e^+e^- \rightarrow \Lambda\bar{\Lambda}$ and $e^+e^- \rightarrow \Lambda\bar{\Lambda}\pi^+\pi^-$

We also inspect the scatter plots of $M_{p\pi^-}$ versus $M_{\bar{p}\pi^+}$ from the selected $p\bar{p}\pi^+\pi^-$ and $p\bar{p}2(\pi^+\pi^-)$ events for studying $e^+e^- \rightarrow \Lambda\bar{\Lambda}$ and $e^+e^- \rightarrow \Lambda\bar{\Lambda}\pi^+\pi^-$. They are shown in Fig. 5. In each figure, the mass window of $\pm 3\sigma_{M_{p\pi^-/\bar{p}\pi^+}}$ (10 MeV/ c^2) around the $\Lambda/\bar{\Lambda}$ nominal mass is taken as the $\Lambda/\bar{\Lambda}$ signal region. Here, $\sigma_{M_{p\pi^-/\bar{p}\pi^+}}$ is the $\Lambda/\bar{\Lambda}$ mass resolution determined by Monte Carlo simulation. In the signal regions, there is 0(3) and 0(1) signal event for the $\Lambda\bar{\Lambda}$ ($\Lambda\bar{\Lambda}\pi^+\pi^-$) final state observed from the $\psi(3770)$ resonance data and the continuum data, respectively.

V. BACKGROUND SUBTRACTION

For the selected candidate events, there are still the contributions from J/ψ and $\psi(3686)$ decays due to ISR

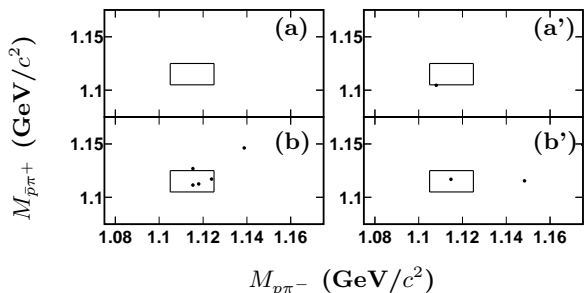


Fig. 5: The scatter plots of $M_{p\pi^-}$ versus $M_{p\pi^+}$ from the selected (a) $p\bar{p}\pi^+\pi^-$ and (b) $p\bar{p}2(\pi^+\pi^-)$ events from the $\psi(3770)$ resonance data (left) and the continuum data (right), where the rectangle regions show the Λ and $\bar{\Lambda}$ signal regions.

returns, the contributions from the other final states due to misidentifying a π as a K or reverse, and the contributions from $D\bar{D}$ decays. The number N_b of these contributions should be subtracted from the number N^{obs} of the candidate events for $e^+e^- \rightarrow f$ (f represents exclusive light hadron final state). These are estimated by Monte Carlo simulation, which has been described in detail in Ref. [10]. Monte Carlo study shows that the other contributions from the decays $\psi(3770) \rightarrow J/\psi\pi^+\pi^-$, $\psi(3770) \rightarrow J/\psi\pi^0\pi^0$, $\psi(3770) \rightarrow J/\psi\pi^0$, $\psi(3770) \rightarrow \gamma\chi_{cJ}$ ($J = 0, 1, 2$) can be neglected [10]. For the $K^+K^-\pi^+\pi^-$ and $K^+K^-2(\pi^+\pi^-)[\pi^0]$ final states, even though we have removed the main contributions from $D\bar{D}$ decays in the previous event selection (see section III), there are still some events from $D\bar{D}$ decays satisfying the selection criteria for the light hadron final states. The number of these events should also be further removed based on Monte Carlo simulation.

After the background subtraction, we obtain the net numbers of the signal events, N^{net} , for some final states. For the other final states, only a few events are observed from the data. We set the upper limits N^{up} on these numbers of the signal events by using the Feldman-Cousins method [22] in the absence of background at 90% confidence level (C.L.). The numbers of N^{obs} , N^b and N^{net} (or N^{up}) are summarized in Tabs. 1 and 2.

VI. RESULTS

A. Monte Carlo efficiency

The detection efficiency ϵ for $e^+e^- \rightarrow$ exclusive light hadrons is estimated by Monte Carlo simulation for the BESII detector [23]. The Monte Carlo events are generated by using a phase space generator including initial state radiation and vacuum polarization corrections [24] with $1/s$ cross section energy dependence. Final state radiation [25] decreases the detection efficiency not more than 0.5%. The generator was used to determine detec-

tion efficiency for $e^+e^- \rightarrow$ exclusive light hadrons in our previous work [10]. Detailed analysis gives the detection efficiency for each final state at $\sqrt{s} = 3.773$ and 3.650 GeV, as shown in the fifth columns of Tabs. 1 and 2. For the modes containing intermediate resonances in the final states, the detection efficiencies listed in the tables do not include the branching fractions for the decays of the intermediate resonances.

B. Systematic error

The systematic error in the measurement of the observed cross section for the exclusive light hadron production arises mainly from the uncertainties in the integrated luminosity of the data set ($\sim 2.1\%$ [3, 4]), the photon selection ($\sim 2.0\%$ per photon), the tracking efficiency ($\sim 2.0\%$ per track), the particle identification ($\sim 0.5\%$ per pion or kaon, $\sim 2.0\%$ per proton), the kinematic fit ($\sim 1.5\%$), the Monte Carlo statistics ($\sim (0.7\sim 5.0)\%$), the branching fractions quoted from PDG [21] ($\sim 0.03\%$ for $\mathcal{B}(\pi^0 \rightarrow \gamma\gamma)$ and $\sim 0.78\%$ for $\mathcal{B}(\Lambda \rightarrow p\pi^-)$), the background subtraction ($\sim (0.0\sim 3.5)\%$), the fit to mass spectrum ($\sim (1.9\sim 13.2)\%$), and the Monte Carlo modeling ($\sim 6.0\%$ [10]). The total systematic error Δ_{sys} for each final state is obtained by adding these uncertainties in quadrature. They are summarized in the sixth columns of Tabs. 1 and 2.

C. Observed cross sections for some final states

The observed cross section for $e^+e^- \rightarrow f$ is obtained by dividing the number N^{net} of the signal events by the integrated luminosity \mathcal{L} of the data set and the detection efficiency ϵ (and the branching fraction \mathcal{B}_i for the possible intermediate resonance decay i containing in some final states),

$$\sigma_{e^+e^- \rightarrow f} = \frac{N^{\text{net}}}{\mathcal{L} \times \epsilon (\times \prod_i^n \mathcal{B}_i)}, \quad (1)$$

where the n is the number of the intermediate resonances in the final state, the \mathcal{B}_i denotes $\mathcal{B}(\pi^0 \rightarrow \gamma\gamma)$, $\mathcal{B}(\rho^0 \rightarrow \pi^+\pi^-)$, $\mathcal{B}(K^{*0} \rightarrow K^+\pi^-)$ or $\mathcal{B}(\Lambda \rightarrow p\pi^-)$ [21]. Inserting the numbers of N^{net} , \mathcal{L} , ϵ (and \mathcal{B}_i) in Eq. (1), we obtain $\sigma_{e^+e^- \rightarrow f}$ for some final states at $\sqrt{s} = 3.773$ and 3.650 GeV, respectively. They are shown in the last columns of Tabs. 1 and 2, where the first error is statistical and the second systematic.

D. Upper limits on observed cross sections for the other final states

For the other final states, only a few events are observed from the data. The upper limit on the observed

cross section for $e^+e^- \rightarrow f$ is set by

$$\sigma_{e^+e^- \rightarrow f}^{\text{up}} = \frac{N^{\text{up}}}{\mathcal{L} \times \epsilon \times (1 - \Delta_{\text{sys}}) (\times \prod_i^n \mathcal{B}_i)}, \quad (2)$$

where N^{up} is the upper limit on the number of the signal events for the final state and Δ_{sys} is the systematic error in the measurement of the observed cross section. Inserting the numbers of N^{up} , \mathcal{L} , ϵ , Δ_{sys} (and \mathcal{B}_i) in Eq. (2), we obtain $\sigma_{e^+e^- \rightarrow f}^{\text{up}}$ for these final states at $\sqrt{s} = 3.773$ and 3.650 GeV, respectively. They are also shown in the last columns of Tabs. 1 and 2.

E. Upper limits on the observed cross sections and the branching fractions for $\psi(3770) \rightarrow f$

With the measured observed cross sections $\sigma_{e^+e^- \rightarrow f}^{3.773 \text{ GeV}}$ and $\sigma_{e^+e^- \rightarrow f}^{3.650 \text{ GeV}}$ for $e^+e^- \rightarrow f$ at $\sqrt{s} = 3.773$ and 3.650 GeV, as listed in Tabs. 1 and 2, we determine the observed cross section for $\psi(3770) \rightarrow f$ by

$$\sigma_{\psi(3770) \rightarrow f} = \sigma_{e^+e^- \rightarrow f}^{3.773 \text{ GeV}} - f_{\text{co}} \times \sigma_{e^+e^- \rightarrow f}^{3.650 \text{ GeV}}, \quad (3)$$

where f_{co} is the coefficient due to the $1/s$ dependence of the cross section. Here, we ignore the possible interference effects between the continuum and resonance amplitudes, and neglect the difference of the vacuum polarization corrections at the two energy points. These yield $\sigma_{\psi(3770) \rightarrow f}$ for each mode, as shown in the second column of Tab. 3, where the first error is the statistical, the second is the independent systematic arising from the uncertainties in the Monte Carlo statistics, in fitting to the mass spectrum and in the background subtraction, and the third is the common systematic error arising from the other uncertainties as discussed in the subsection B. For the final states with a few signal events observed from the continuum data, such as $2(K^+K^-)\pi^+\pi^-$ and $4(\pi^+\pi^-)\pi^0$, etc., we neglect their contributions from the continuum production in the determination of $\sigma_{\psi(3770) \rightarrow f}$.

The upper limits on the observed cross sections, $\sigma_{\psi(3770) \rightarrow f}^{\text{up}}$, for $\psi(3770)$ decay to $4(\pi^+\pi^-)\pi^0$, $\Lambda\bar{\Lambda}$ and $\Lambda\bar{\Lambda}\pi^+\pi^-$ are directly set based on the upper limits on their observed cross sections at 3.773 GeV. While, for the other final states, the $\sigma_{\psi(3770) \rightarrow f}^{\text{up}}$ is set through shifting the cross section by 1.64σ , where σ is the total error of the measured cross section. For the $\rho^0 K^+K^-$ and $\rho^0 p\bar{p}$ final states, the central values of $\sigma_{\psi(3770) \rightarrow f}$ are less than zero. In this case, we treat them as zero and then set their upper limits. The results on $\sigma_{\psi(3770) \rightarrow f}^{\text{up}}$ are summarized in the third column of Tab. 3.

The upper limit on the branching fraction for $\psi(3770) \rightarrow f$, $\mathcal{B}_{\psi(3770) \rightarrow f}^{\text{up}}$, is set by dividing its upper limit on the observed cross section $\sigma_{\psi(3770) \rightarrow f}^{\text{up}}$ by the observed cross section $\sigma_{\psi(3770)}^{\text{obs}}$ for the $\psi(3770)$ production at 3.773 GeV and a factor $(1 - \Delta\sigma_{\psi(3770)}^{\text{obs}})$, where

$\Delta\sigma_{\psi(3770)}^{\text{obs}}$ is the total relative error of the $\sigma_{\psi(3770)}^{\text{obs}}$. Here, $\sigma_{\psi(3770)}^{\text{obs}} = (7.15 \pm 0.27 \pm 0.27)$ nb [10], is obtained by weighting the two measurements [4, 26] from BES Collaboration. The results on $\mathcal{B}_{\psi(3770) \rightarrow f}^{\text{up}}$ are shown in the last column of Tab. 3. The upper limits on the observed cross sections and the branching fractions for $\psi(3770) \rightarrow \Lambda\bar{\Lambda}$ and $\psi(3770) \rightarrow \Lambda\bar{\Lambda}\pi^+\pi^-$ are consistent with the measurements [13] from CLEO Collaboration.

VII. SUMMARY

In summary, by analyzing the data sets taken at $\sqrt{s} = 3.773$ and 3.650 GeV with the BESII detector at the BEPC collider, we have measured the observed cross sections for 12 exclusive light hadron final states produced in e^+e^- annihilation at the two energy points. With the measured observed cross sections at the two energy points, we set the upper limits on the observed cross sections and the branching fractions for $\psi(3770)$ decay to these final states at 90% C.L. In the measurements, we ignore the interference effects between the continuum and resonance amplitudes due to not knowing the details about the two amplitudes. In this case, even though we have not observed significant difference between the observed cross sections for most light hadron final states at the two energy points, we still can not conclude that the $\psi(3770)$ does not decay into these final states. To extract the branching fractions for $\psi(3770) \rightarrow$ exclusive light hadrons, a better way is to analyze their energy-dependent observed cross sections at more energy points covering both $\psi(3770)$ and $\psi(3686)$ [27]. However, these observed cross sections reported in this Letter and those reported in Ref. [10], would be valuable to get better comprehensions for both the mechanism of the continuum light hadron production and the discrepancy between the observed cross sections for $D\bar{D}$ and $\psi(3770)$ production.

VIII. ACKNOWLEDGMENTS

The BES collaboration thanks the staff of BEPC for their hard efforts. This work is supported in part by the National Natural Science Foundation of China under contracts Nos. 10491300, 10225524, 10225525, 10425523, the Chinese Academy of Sciences under contract No. KJ 95T-03, the 100 Talents Program of CAS under Contract Nos. U-11, U-24, U-25, the Knowledge Innovation Project of CAS under Contract Nos. U-602, U-34 (IHEP), the National Natural Science Foundation of China under Contract No. 10225522 (Tsinghua University).

Tab. 1: The observed cross sections for $e^+e^- \rightarrow$ exclusive light hadrons at $\sqrt{s} = 3.773$ GeV, where N^{obs} is the number of events observed from the $\psi(3770)$ resonance data, N^{b} is the total number of background events, N^{net} is the number of the signal events, N^{up} is the upper limit on the number of the signal events, ϵ is the detection efficiency, Δ_{sys} is the relative systematic error in the measurement of the observed cross section, σ is the observed cross section and σ^{up} is the upper limit on the observed cross section set at 90% C.L.

$e^+e^- \rightarrow$	N^{obs}	N^{b}	N^{net} (or N^{up})	ϵ [%]	Δ_{sys}	σ (or σ^{up}) [pb]
$K^+K^-2(\pi^+\pi^-)$	92.7 ± 9.7	3.2 ± 0.5	89.5 ± 9.7	3.08 ± 0.06	0.141	$168.0 \pm 18.2 \pm 23.7$
$2(K^+K^-)\pi^+\pi^-$	5.0 ± 2.3	0.3 ± 0.1	4.7 ± 2.3	2.29 ± 0.05	0.143	$11.9 \pm 5.8 \pm 1.7$
$p\bar{p}2(\pi^+\pi^-)$	24.0 ± 4.9	0.9 ± 0.2	23.1 ± 4.9	5.69 ± 0.08	0.150	$23.5 \pm 5.0 \pm 3.5$
$4(\pi^+\pi^-)$	50.0 ± 7.1	1.9 ± 0.3	48.1 ± 7.1	2.11 ± 0.05	0.179	$131.8 \pm 19.5 \pm 23.6$
$K^+K^-2(\pi^+\pi^-)\pi^0$	21.3 ± 5.0	3.1 ± 0.6	18.2 ± 5.0	0.46 ± 0.02	0.160	$231.5 \pm 63.6 \pm 37.0$
$4(\pi^+\pi^-)\pi^0$	6	0	< 11.47	0.40 ± 0.02	0.189	< 206.9
$\rho^0\pi^+\pi^-$	330.1 ± 37.4	10.4 ± 1.9	319.7 ± 37.4	16.52 ± 0.26	0.117	$111.9 \pm 13.1 \pm 13.1$
$\rho^0K^+K^-$	50.0 ± 14.4	7.1 ± 1.5	42.9 ± 14.4	7.26 ± 0.12	0.128	$34.2 \pm 11.5 \pm 4.4$
$\rho^0p\bar{p}$	41.6 ± 10.1	0.3 ± 0.1	41.3 ± 10.1	18.25 ± 0.14	0.141	$13.1 \pm 3.2 \pm 1.8$
$K^{*0}K^-\pi^+ + c.c.$	84.3 ± 13.6	1.0 ± 0.2	83.3 ± 13.6	7.63 ± 0.12	0.110	$94.7 \pm 15.5 \pm 10.4$
$\Lambda\bar{\Lambda}$	0	0	< 2.44	15.77 ± 0.13	0.116	< 2.5
$\Lambda\bar{\Lambda}\pi^+\pi^-$	3	0	< 7.42	4.63 ± 0.07	0.150	< 26.7

Tab. 2: The observed cross sections for $e^+e^- \rightarrow$ exclusive light hadrons at $\sqrt{s} = 3.650$ GeV, where N^{obs} is the number of events observed from the continuum data, and the definitions of the other symbols are the same as those in Tab. 1.

$e^+e^- \rightarrow$	N^{obs}	N^{b}	N^{net} (or N^{up})	ϵ [%]	Δ_{sys}	σ (or σ^{up}) [pb]
$K^+K^-2(\pi^+\pi^-)$	30.0 ± 5.5	0.1 ± 0.0	29.9 ± 5.5	2.79 ± 0.05	0.141	$164.9 \pm 30.3 \pm 23.2$
$2(K^+K^-)\pi^+\pi^-$	2	0	< 5.91	2.16 ± 0.05	0.142	< 49.1
$p\bar{p}2(\pi^+\pi^-)$	8.0 ± 2.9	0.1 ± 0.0	7.9 ± 2.9	5.33 ± 0.07	0.150	$22.8 \pm 8.4 \pm 3.4$
$4(\pi^+\pi^-)$	10.0 ± 3.2	0.0 ± 0.0	10.0 ± 3.2	2.02 ± 0.04	0.179	$76.2 \pm 24.4 \pm 13.6$
$K^+K^-2(\pi^+\pi^-)\pi^0$	5.4 ± 2.5	0.0 ± 0.0	5.4 ± 2.5	0.56 ± 0.02	0.150	$150.2 \pm 69.5 \pm 22.5$
$4(\pi^+\pi^-)\pi^0$	0	0	< 2.44	0.39 ± 0.01	0.184	< 119.4
$\rho^0\pi^+\pi^-$	133.5 ± 24.4	3.3 ± 0.8	130.2 ± 24.4	17.63 ± 0.28	0.115	$113.6 \pm 21.3 \pm 13.1$
$\rho^0K^+K^-$	30.4 ± 8.8	2.0 ± 0.6	28.4 ± 8.8	7.58 ± 0.12	0.110	$57.6 \pm 17.9 \pm 6.3$
$\rho^0p\bar{p}$	22.2 ± 7.8	0.0 ± 0.0	22.2 ± 7.8	19.32 ± 0.14	0.157	$17.7 \pm 6.2 \pm 2.8$
$K^{*0}K^-\pi^+ + c.c.$	29.5 ± 9.0	0.2 ± 0.1	29.3 ± 9.0	7.91 ± 0.12	0.169	$85.5 \pm 26.3 \pm 14.4$
$\Lambda\bar{\Lambda}$	0	0	< 2.44	16.97 ± 0.13	0.116	< 6.1
$\Lambda\bar{\Lambda}\pi^+\pi^-$	1	0	< 4.36	4.51 ± 0.07	0.150	< 42.9

-
- [1] G. Rong, D. H. Zhang, J. C. Chen, hep-ex/0506051.
[2] CLEO Collaboration, D. Besson, et al., Phys. Rev. Lett. **96** (2006) 092002.
[3] BES Collaboration, M. Ablikim et al., Phys. Lett. **B 641** (2006) 145.
[4] BES Collaboration, M. Ablikim et al., Phys. Rev. Lett. **97** (2006) 121801.
[5] Particle Data Group, 2007 partial updata for edition 2008 (URL:http://pdg.lbl.gov).
[6] BES Collaboration, J. Z. Bai et al., HEP & NP **28(4)** (2004) 325.
[7] BES Collaboration, M. Ablikim et al., Phys. Lett. **B 605** (2005) 63.
[8] BES Collaboration, M. Ablikim et al., Phys. Rev. **D 70** (2004) 077101.
[9] BES Collaboration, M. Ablikim et al., Phys. Rev. **D 72** (2005) 072007.
[10] BES Collaboration, M. Ablikim et al., arXiv: 0705.2276[hep-ex], Phys. Lett. **B 650** (2007) 111.
[11] CLEO Collaboration, N. E. Adam et al., Phys. Rev. Lett. **96** (2006) 082004.
[12] CLEO Collaboration, T. E. Coans et al., Phys. Rev. Lett. **96** (2006) 182002.
[13] CLEO Collaboration, G. S. Huang et al., Phys. Rev. Lett. **96** (2006) 032003.
[14] CLEO Collaboration, G. S. Adams et al., Phys. Rev. **D 73** (2006) 012002.
[15] CLEO Collaboration, D. Cronin-Hennessy et al., Phys. Rev. **D 74** (2006) 012005.
[16] CLEO Collaboration, R. A. Briere et al., Phys. Rev. **D**

Tab. 3: The upper limits on the observed cross section $\sigma_{\psi(3770)\rightarrow f}^{\text{up}}$ and the branching fraction $\mathcal{B}_{\psi(3770)\rightarrow f}^{\text{up}}$ for $\psi(3770) \rightarrow f$ are set at 90% C.L. The $\sigma_{\psi(3770)\rightarrow f}$ in the second column is calculated with Eq. (3), where the first error is the statistical, the second is the independent systematic, and the third is the common systematic error. Here, the upper ^t denotes that we treat the upper limit on the observed cross section for $e^+e^- \rightarrow f$ at 3.773 GeV as $\sigma_{\psi(3770)\rightarrow f}^{\text{up}}$, the upper ⁿ denotes that we neglect the contribution from the continuum production, and the upper ^z denotes that we treat the central value of $\sigma_{\psi(3770)\rightarrow f}$ as zero if it is less than zero.

Decay Mode	$\sigma_{\psi(3770)\rightarrow f}$ [pb]	$\sigma_{\psi(3770)\rightarrow f}^{\text{up}}$ [pb]	$\mathcal{B}_{\psi(3770)\rightarrow f}^{\text{up}}$ [$\times 10^{-3}$]
$K^+K^-2(\pi^+\pi^-)$	$13.7 \pm 33.7 \pm 4.4 \pm 1.9$	< 69.5	< 10.3
$2(K^+K^-)\pi^+\pi^-$	$11.9 \pm 5.8 \pm 0.4 \pm 1.7^n$	< 21.8	< 3.2
$p\bar{p}2(\pi^+\pi^-)$	$2.2 \pm 9.3 \pm 0.5 \pm 0.3$	< 17.5	< 2.6
$4(\pi^+\pi^-)$	$60.5 \pm 30.0 \pm 3.6 \pm 10.7$	< 113.1	< 16.7
$K^+K^-2(\pi^+\pi^-)\pi^0$	$90.9 \pm 91.0 \pm 16.1 \pm 13.2$	< 244.0	< 36.0
$4(\pi^+\pi^-)\pi^0$	$< 206.9^{tn}$	< 206.9	< 30.6
$\rho^0\pi^+\pi^-$	$5.6 \pm 23.9 \pm 7.6 \pm 0.6$	< 46.6	< 6.9
$\rho^0K^+K^-$	$-19.7 \pm 20.3 \pm 3.1 \pm 2.1^z$	< 33.9	< 5.0
$\rho^0p\bar{p}$	$-3.5 \pm 6.6 \pm 2.1 \pm 0.4^z$	< 11.4	< 1.7
$K^{*0}K^-\pi^+ + c.c.$	$14.7 \pm 29.1 \pm 11.1 \pm 1.5$	< 65.8	< 9.7
$\Lambda\bar{\Lambda}$	$< 2.5^{tn}$	< 2.5	< 0.4
$\Lambda\bar{\Lambda}\pi^+\pi^-$	$< 26.7^{tn}$	< 26.7	< 3.9

- 74 (2006) 031106.
- [17] BES Collaboration, J. Z. Bai et al., Nucl. Instrum. Methods **A 344** (1994) 319.
- [18] BES Collaboration, J. Z. Bai et al., Nucl. Instrum. Methods **A 458** (2001) 627.
- [19] BES Collaboration, M. Ablikim et al., Phys. Lett. **B 597** (2004) 39;
BES Collaboration, M. Ablikim et al., Phys. Lett. **B 603** (2004) 130;
BES Collaboration, M. Ablikim et al., Phys. Lett. **B 608** (2005) 24.
- [20] BES Collaboration, M. Ablikim et al., Nucl. Phys. **B 727** (2005) 395.
- [21] Particle Data Group, W.-M. Yao, et al., J. Phys. **G 33** (2006) 1.
- [22] G. J. Feldman and R. D. Cousins, Phys. Rev. **D 57** (1998) 3873.
- [23] BES Collaboration, M. Ablikim et al., Nucl. Instrum. Methods **A 552** (2005) 344.
- [24] E. A. Kuraev and V. S. Fadin, Yad. Fiz. **41** (1985) 377.
- [25] E. Barberio, Z. Was, Comput. Phys. Commun. **79** (1994) 291.
- [26] BES Collaboration, M. Ablikim et al., hep-ex/0612056, Phys. Lett. **B** in press.
- [27] G. Rong (For BES Collaboration), Int. J. Mod. Phys. **A 21** (2006) 5416.